IRAQI JOURNAL OF APPLIED PHYSICS
Vol. 19, No. 4B, November 2023, pp. 167-170

Lara S. Khalil
Mazin A. Alalousi

Department of Physics, College of Science, University of Anbar, Ramadi, IRAQ

Preparation and Characterization of Fullerene/AuNPs Composite Films

This study aims to prepare fullerene/gold nanoparticles composite by electrospray and investigate the influence of the gold nanoparticles concentration of 0.412, 1.944, and 3.575 ppm on the film structural, morphological, and Raman properties. XRD patterns demonstrated initial changes in the structural phases, where the increasing of AuNPs concentration led to decrease of C_{60} phases and increase of both C_{60}-polymaric and C_{70} phases. Moreover, the field emission electron microscope images evident a variation in size distribution, formation, and phase patterns with the AuNPs concentration. Raman spectra demonstrated the formation of fullerenes C_{60}, C_{60} polymer, and C_{70} with appearance of the characteristic vibrational modes of these fullerenes $H_g^{(1)}$, $F_{2g}^{(1)}$, and $A_g^{(2)}$.

Keywords: Fullerene; Laser ablation; Wasted batteries; Raman spectroscopy
Received: 06 August 2023; **Revised:** 28 August 2023; **Accepted:** 30 August 2023

1. Introduction

Fullerenes are distinguished by their highly symmetrical cage-like spherical shape, which aroused much interest for this reason [1]. Additionally, these structures have infinitesimal sizes and adopt various shapes within a fully or partially enclosed carbon net. These structures consist of carbon atoms connected by single or double bonds, often forming rings comprising 5 to 7 atoms. Their closed structure can be represented by the formula C_n, where *n* corresponds to the number of carbon atoms involved. Notably, graphene serves as the fundamental building block for all raw materials that give rise to fullerenes [2]. Due to their unique chemical and physical properties such as their affinity with carbonic compounds, noble metals, other materials, controlled optical gaps, and electronic structure were nominated for entry into several applications [3]. Recently, new trends for fullerenes in biomedical uses have emerged [4-6], pharmacology, and photocatalysis applications [7]. Therefore, made the reactivity of fullerenes is an area of immense interest in the synthetic organic chemistry field [8]. Despite the importance of entering this type of carbon in many applications and causing breakthroughs in some industries, there are many challenges, including challenges in its manufacture and production, as the quantities of fullerene produced were not sufficient to be used in many applications in addition to its high cost [9-11]. There are four our main routes for the fullerenes synthesis; laser irradiation of carbon, laser irradiation of poly aromatic hydrocarbon, electrical arc graphene heating, and resistive arc graphene heating [12]. Recently, Alani and Alalousi succeeded in producing carbon particles colloidal through the utilization of an Nd-YAG laser. These particles were then electrostatically sprayed to directly obtain fullerene films [13]. One of the methods used in the previous C60 configuration Carbon types, especially C60 and C70, are characterized by Raman spectroscopy by calculating their vibrational patterns depending on the form of their unified bonds, which are carbon-carbon (C-C) bonds [1].

Gold and silver nanoparticles are considered to have a great effect in improving the surface, which aims to enhance the Raman spectra, where the surface plasmon resonance absorption of gold nanoparticles on the surface contributes to strengthening and strengthening that very surface. This technique is called Surface-Enhanced Raman Scattering (SERS) because these particles are the mineral has a distinctive nanostructure that contributes to the detection of particles [14,15].

This study aims to prepare and study the effect of gold nanoparticles (AuNPs) concentration on the structural, morphological, and Raman spectroscopic of the prepared fullerene/ AuNPs films based on dry batteries.

2. Experimental Part

A colloidal carbon solution was prepared according to previous study [13]. A carbon target was placed in a beaker containing 50 mL of deionized water and irradiated by a pulsed Nd:YAG laser with (λ=1064 nm, 100 mJ of energy, 6 Hz of pulses rate, and 6000 pulses). The distance between the surface of pellet and the laser lens was 12 cm. Then, the gold colloidal was prepared in the same laser parameters with (0.412, 1.944, and 3.575) ppm of concentration, respectively. The color of the water began to change to a light purple color. As well, mixtures of carbon/AuNPs colloidal were prepared by irradiating

of target into AuNPs colloidal (50 ml) with 1000, 2000, and 3000 pulses. To fabricate fullerene and fullerene/AuNPs films, each colloidal was sprayed separately after filtration on quartz using an electrospray device. The nozzle biased positively while the substrates biased negatively with DC 5 KV as a bias potential, additional to 250±25°C of substrates temperature.

Characterization: Structural properties were chartered by analysis of X-ray diffraction (XRD) patterns (x-ray CuKα radiation and accelerated voltage of 40 kV). Williamson-Hall relation was [13] applied to estimate the crystalline size

$$D_{hkl} = \left(\frac{A\lambda}{cos\theta.\beta_{hkl}}\right) + (4\varepsilon \sin\theta) \qquad (1)$$

FE-SEM images achieved via field emission scanning electron microscope (FE-SEM, INSPECT-550) have been used to evaluate the morphological properties of the prepared film surfaces, addition to the energy dispersive x-ray (EDX) microanalysis to estimate elemental analysis associated with the prepared films, as well Raman spectra were achieved to detect their vibrational and rotational.

3. Results and discussion

XRD patterns have been analyzed based on ICSD 98-060-2518, ICSD 98-007-5506, ICSD 98-009-5370, and ICSD 98-005-6668 cards. Pure carbon films showed a polycrystalline structure with the dominance of C_{60} phases at 2θ of approximately 15.29°, 20.77°, 37.77°, 39.25°, and 50.8663°. The dominant phase was observed at about 20.77° (311) with crystallite size found at about 80.76 nm. Likewise, the presence of two main phases, C_{70} and C_{60}- Polymer but with lower attributions as shown in Fig. (1).

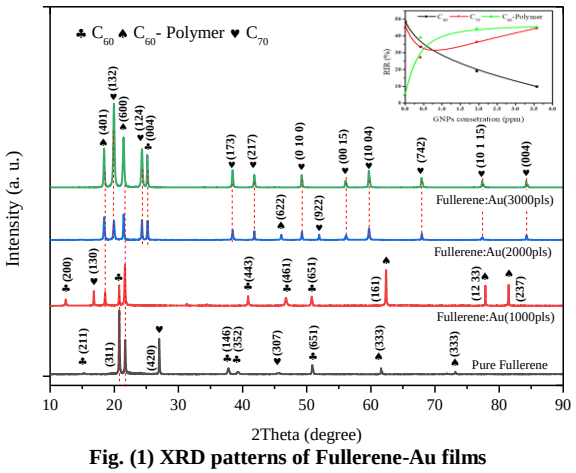

Fig. (1) XRD patterns of Fullerene-Au films

Notably, the introduction of AuNPs indicates their influence on the distribution of diffraction phases, which led to the dominant phase shift (600) at 2θ = 21.65° (C_{70}) with crystallite size about 68 nm when AuNPs prepared with concentration of 0.412 ppm, In the meantime, the dominant phase (600) shifted by approximately 0.202°, and the lattice stress decreased by around 0.207. These changes are likely a result of the crystalline potentials influenced by the increased concentration of the C_{60}-polymer phase when the AuNPs concentration was raised to 1.944 ppm. In contrast, the dominant phase shifted to (132) at 19.9° (C_{70}), which can be attributed to the AuNPs concentration reaching 3.575 ppm. As for the quantitative intensity calculated using the (RIR) method, it was observed that the C_{60}-polymer exhibited a clear increase with the rising concentration of AuNPs as shown in thumbnail chart in Fig. (1), indicating their role as nucleation centers. Table (1) demonstrates the dominant phases of the fullerene and fullerene/AuNPs films XRD patterns.

Figure (2) represents FE-SEM images that mainly give morphological information about the surface of the prepared fullerenes and AuNPs-fullerene composite films with 0, 0.412, 1.944, and 3.575 ppm.

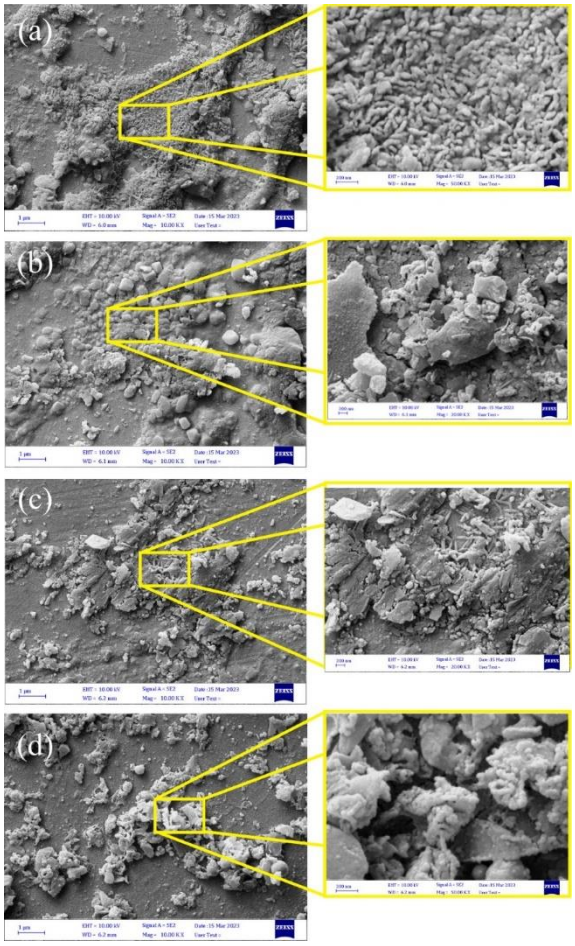

Fig. (2) FE-SEM images of the prepared fullerenes and AuNPs-fullerene composite films with 0.412, 1.944, and 3.575 ppm

Notably, a distinct separation can be observed among the various particles, particularly nanorods (that are believed to be C_{60}-polymeric can be known as nanowhiskers (C_{60}FNWs) [16]) with an average diameter of approximately 39 nm, as depicted in Fig. (2a). The particle separation and the non-uniformity of their distribution can be attributed to the

 ISSN (print) 1813-2065, (online) 2309-1673

phenomenon of impurity segregation due to variations in the surface energy of these different particles [17]. The addition of AuNPs have led to a clear change in the phases of the composition of the prepared films, where the addition of gold with a concentration of 0.412 and 1.944 ppm led to a variety of formations consisting of a shell-like formation consisting of aggregated spherical particles with average size about 11 nm. In addition, find rods with an average diameter of about 51 nm, which are thought to go back either to gold or as an accidental product with carbon nanotubes. With regard to the visible cracks in the ground, they are believed to be caused by the effect of both substrate temperature and surface energy. This is due to the film formation mechanism, where it is likely to be a surface density of the product from the effect of uneven heat distribution due to differing thickness of membrane areas and heterogeneous surface energy. The increase in the concentration of AuNPs to 3.575 ppm led to the emergence of the so-called segregation of impurity phenomena, formations similar to cauliflower flower as shown in Fig. (2c).

One of the active techniques to characterization of the carbon structures is Raman spectroscopy [18]. At high symmetry of fullerenes (C_{60} and C_{70}) has numerous vibrational modes, where are ten modes for C_{60} and 53 modes for C_{70} [19]. $A_g^{(2)}$, $H_g^{(1)}$, $H_g^{(7)}$, and $Hg^{(8)}$ are the apparent mean vibrational modes in C_{60} spectra [1]. In fact, $Ag^{(2)}$ mode, which is non-degenerate and the strongest among the Raman-active $Ag^{(2)}$) modes in addition to $Hg^{(8)}$ of C_{60}, has frequently been utilized to characterize C_{60} solids, these two modes and $Hg^{(7)}$ that related to pentagon shear [20], while some theoretical studies exceed this limit [21]. The $Ag^{(2)}$ mode peak position of accurately reflects the physical state of C_{60} molecules [16].

However, in Fig. (3), the Raman spectra of fullerene and fullerene/AuNPs films can be seen. The spectra included peaks for different modes with varying shifts and intensities according to the concentration of gold compared to what was reported previously in numerous of literature because of these films containing structural phases as observed in the X-ray diffraction patterns. All spectra showed the strong appearance of the peaks that represent $H_g^{(1)}$ mode [22], starting at the wavenumber 288 cm^{-1}, which is observed to shift to the right and increase in intensity with increasing gold concentration. This change in location and intensity is attributed to the effect of the crystal field resulting from the polymerization of C_{60} and the increase in chains length that occurs during the formation of nanopeapod [23]. In the meanwhile, $F_{2g}^{(1)}$ represented at wavenumber of 644 cm^{-1} which associated with internal active Raman mode of C_{60} molecule I_h polarization, that suffered of downshifting due to varying in the rotation factor [24]. The weak peak at 897 cm^{-1} is a non-Raman active mode, but it shows oscillation in position, intensity, and broadening (FWHM) as the concentration of AuNPs increases., where upshift to 910, 920.6, then downshift to 908 cm^{-1} with increasing of AuNPs concentration. Furthermore, the pentagonal pinch mode associated with the $Ag^{(2)}$ mode for both C^{60} and C^{70} is strongly visible at 1449 cm^{-1}, which suffers intensity increases with the volume fraction for C^{70} increasing. This peak is important in determining the molecular structure of fullerenes as it relates to the vibration of the five-ring present in fullerenes [8,25,26]. The graphite may be contributed several weak peaks at 1930, 2145, 3009, 3282, 4015, 4272 cm^{-1}, including the characterized peak 2079 cm^{-1}, which is related to 2D (or as originally known G'), the distortion and deflection that this peak suffers from results from disturbances in the vibration mode as a result of the field potential factors of the surrounding crystals [27].

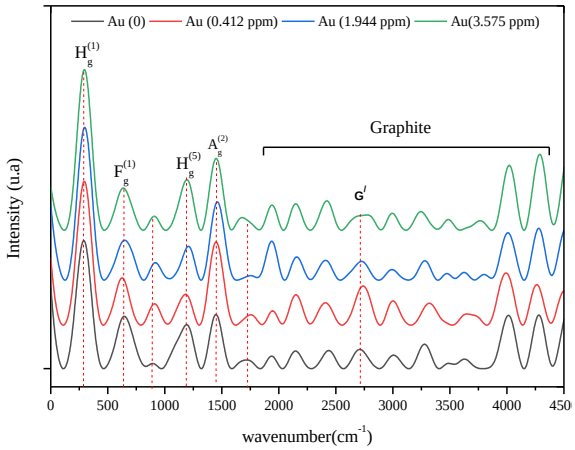

Fig. (3) Raman spectra of the prepared fullerenes and AuNPs-fullerene composite films with 0.412, 1.944, and 3.575 ppm

4. Conclusions

Graphite parts of wasted batteries can be utilized as precursors to prepare the fullerenes materials. These materials were effectively created in the form of thick films utilizing pulsed laser ablation and electrospray techniques successfully, containing C_{60}, C_{70}, and C_{60}-polymer structures. Concentration of AuNPs in fullerene/AuNPs influenced the structural properties of the prepared films, which led to the transit of most C_{60} structure to C_{70}, and C_{60}-polymer structures with increasing of AuNPs concentration. This applies to both morphological characteristics and enhanced Raman spectra.

References

[1] D. Jing and Z. Pan, "Molecular vibrational modes of C_{60} and C_{70} via finite element method", *Eur. J. Mech. A: Solids*, 28 (2009) 948–954.

[2] N. Ota, "Graphene Molecule Compared With Fullerene C_{60} As Circumstellar Carbon Dust Of Planetary Nebula", *ArXiv Astrophys.*, 1904 (2019) 1-9.

[3] C. Ji et al., "Recent Developments of Carbon Dots in Biosensing: A Review", *ACS Sensors*, 5

(2020) 2724–2741.
[4] A.B. Gaur et al., "Biomedical Applications of Carbon Nanomaterials: Fullerenes, Quantum Dots, Nanotubes, Nanofibers, and Graphene", *Materials (Basel)*, 14 (2021) 5978.
[5] N. Mulqueen, K. Sneed and Y. Pathak, "Recent Trends in Fullerenes Biomedical Applications", *Nov. Res. Sci.*, 10 (2022) 000748.
[6] A. Kausar, "Potential of Polymer/Fullerene Nanocomposites for Anticorrosion Applications in the Biomedical Field", *J. Compos. Sci.*, 6 (2022) 1-13.
[7] M.S. Nadeem et al., "Synergistic photocatalytic properties of fullerene (C_{60}) anchored V/Cu dual-doped NiO nanocomposites for water disinfection", *Mater. Sci. Eng. B*, 297 (2023) 116705.
[8] J.B. Kimbrell et al., "Analysis of mixtures of C_{60} and C_{70} by Raman spectrometry", *Nanosci. Meth.*, 3 (2014) 40–46.
[9] J. Sanchís et al., "Transformation of C60 fullerene aggregates suspended and weathered under realistic environmental conditions", *Carbon*, 128 (2018) 54–62.
[10] A.I. Kharlamov, M.E. Bondarenko and N.V. Kirillova, "New method for synthesis of fullerenes and fullerene hydrides from Benzene", *Russian J. Appl. Chem.*, 85 (2012) 233–238.
[11] L.T. Scott, "Methods for the chemical synthesis of fullerenes", *Angew. Chemie - Int. Ed.*, 43 (2004) 4994–5007.
[12] A. Nimibofa et al., "Fullerenes: Synthesis and Applications", *J. Mater. Sci. Res.*, 7 (2018) 22.
[13] B.M.A. Alani and M.A. Alalousi, "Structural, Morphological, and Spectroscopical Properties of Fullerenes (C_{60}) Thin Film Prepared via Electrospray Deposition", *J. Phys. Conf. Ser.*, 1829 (2021).
[14] H. Chu et al., "Decoration of gold nanoparticles on surface-grown single-walled carbon nanotubes for detection of every nanotube by surface-enhanced raman spectroscopy", *J. Am. Chem. Soc.*, 131 (2009) 14310–14316.
[15] D. Roy, S. Kanojia and K. Mukhopadhyay, "Analysis of carbon-based nanomaterials using Raman spectroscopy : principles and case studies", *Bull. Mater. Sci.*, 44 (2021) 1-9.
[16] T. Konno et al., "Precise Raman measurements of C_{60} fullerene nanowhiskers synthesized using the liquid-liquid interfacial precipitation method", *Trans. Mater. Res. Soc. Japan.*, 41 (2016) 289–295.
[17] M.A. Alalousi et al., "Sensing Enhancement of Gold Nanoparticles Doped-TiO_2 Thin Films as H_2S Gas Sensor", *Nano Hybr. Compos.*, 35, (2022) 1–10.
[18] M. Han et al., "PEI-functionalized carbon nanotube thin film sensor for CO_2 gas detection at room temperature", *mdpi Micromach.*, 12(9) (2021) 1053.
[19] H. Chadli, F. Fergani and A. Rahmani, "Structural and Vibrational Properties of C_{60} and C_{70} Fullerenes Encapsulating Carbon Nanotubes", in N. Kamanina (Ed.), **Fullerenes Relat. Mater. Appl.**, IntechOpen (2018) pp. 109-127.
[20] A. Dorner-Reisel et al., "Effect of fullerene C_{60} thermal and tribomechanical loading on Raman signals", *Diam. Relat. Mater.*, 126 (2022) 109036.
[21] N. Khinevich et al., "Surface enhanced Raman spectroscopy of fullerene C_{60} drop-deposited on the silvered porous silicon", *J. Phys. Conf. Ser.*, 917 (2017) 8–12.
[22] H. Chadli, A. Rahmani and J.L. Sauvajol, "Raman spectra of C_{60} dimer and C_{60} polymer confined inside a (10,10) single-walled carbon nanotube", *J. Phys. Cond. Matter*, 22 (2010).
[23] S. Samiullah, "Spectroscopic characterization of fullerenes", Luleå University of Technology (2008).
[24] H. Kuzmany et al., "Raman spectroscopy of fullerenes and fullerene-nanotube composites", *Philos. Trans. R. Soc. London. Ser. A Math. Phys. Eng. Sci.*, 362 (2004) 2375–2406.
[25] R. Saito et al., "Raman spectroscopy of graphene and carbon nanotubes", *Adv. Phys.*, 60 (2011) 413–550.
[26] Z.F. Kadhim, E.M. Saeed and H.A.H. Al-jubouri, "Phases of Deposited Carbon Films By Pulsed Laser Deposition - Review", *Int. J. Mech. Prod. Eng. Res. Develop.*, 10 (2020) 5139–5156.
[27] V. Zólyomi, J. Koltai and J. Kürti, "Resonance Raman spectroscopy of graphite and graphene", *phys. stat. sol. Basic Res.*, 248 (2011) 2435–2444.

Table (1) XRD parameters of the dominant phase for fullerene and fullerene/AuNPs films

AuNPs Conc. (ppm)	2θ (deg)	d (Å)	hkl	FHWM (deg)	Intensity	Crystallite Size (nm)	Lattice strain	Fullerene	Crystalline System
0	20.77	4.28	3 1 1	0.13	52.01	80.73	0.265	C_{60}	Cubic
0.412	21.65	4.10	6 0 0	0.155	44	67.67	0.303	C_{70}	Orthorhombic
1.944	21.45	4.14	6 0 0	0.155	27.74	208.55	0.099	C_{70}	Orthorhombic
3.575	19.93	4.45	1 3 2	0.216	67.72	44	0.506	C_{70}	Orthorhombic

 ISSN (print) 1813-2065, (online) 2309-1673